Impact of impurity-based phonon resonant scattering on thermal conductivity of single crystalline GaN ©

Cite as: Appl. Phys. Lett. 117, 082101 (2020); https://doi.org/10.1063/5.0018824 Submitted: 17 June 2020 . Accepted: 10 August 2020 . Published Online: 24 August 2020

Degah Bagheri, Deramod Reddy, Ji Hyun Kim, Robert Rounds, De Tomasz Sochacki, Ronny Kirste, De Michał Bockowski, Ramón Collazo, and De Zlatko Sitar

COLLECTIONS

F This paper was selected as Featured







ARTICLES YOU MAY BE INTERESTED IN

The nature of the DX state in Ge-doped AlGaN

Applied Physics Letters 116, 222102 (2020); https://doi.org/10.1063/5.0008362

Growth of bulk GaN crystals

Journal of Applied Physics 128, 050902 (2020); https://doi.org/10.1063/5.0009900

Complexes and compensation in degenerately donor doped GaN Applied Physics Letters 117, 102109 (2020); https://doi.org/10.1063/5.0013988





Impact of impurity-based phonon resonant scattering on thermal conductivity of single crystalline GaN •

Cite as: Appl. Phys. Lett. **117**, 082101 (2020); doi: 10.1063/5.0018824 Submitted: 17 June 2020 · Accepted: 10 August 2020 · Published Online: 24 August 2020







Pegah Bagheri,^{1,a)} (D) Pramod Reddy,² (D) Ji Hyun Kim,¹ Robert Rounds,¹ Tomasz Sochacki,³ (D) Ronny Kirste,² Michał Bockowski,³ (D) Ramón Collazo,¹ and Zlatko Sitar^{1,2} (D)

AFFILIATIONS

- Department of Materials Science and Engineering, North Carolina State University, Raleigh, North Carolina 27695, USA
- ²Adroit Materials, 2054 Kildaire Farm Road, Cary, North Carolina 27518, USA
- ³Institute of High-Pressure Physics, Polish Academy of Sciences, Sokołowska 29/37, 01-142 Warsaw, Poland

ABSTRACT

The impact of impurities on the thermal conductivity of halide vapor phase epitaxy gallium nitride (GaN) was studied. Phonon resonances with impurities, modeled as Lorentz oscillators, were used to explain the much lower thermal conductivity than predicted by the Debye–Callaway model. The resonance energies for the oscillators were determined by Raman spectroscopy for Mn and by mass difference approximation for C and Fe. Employing the obtained resonance energies and proportionality factors extracted as fitting parameters, the modified model showed a good agreement with the experimental data. While the doping decreased thermal conductivity for all temperatures, the room temperature values started decreasing significantly once the doping levels approached $\sim 10^{19} \, \mathrm{cm}^{-3}$. Consequently, required doping levels to achieve certain GaN-based devices may reduce the thermal conductivity of GaN by as much as 1/3.

Published under license by AIP Publishing. https://doi.org/10.1063/5.0018824

Single crystal gallium nitride (GaN) as a wide bandgap semiconductor has a broad range of applications in optoelectronics and electronics. 1-3 The demonstration of ideal Schottky and p-n diodes, 4,5 high electron mobility, and low on-resistance, along with a high breakdown field (3.65 MV/cm), make GaN a promising candidate for power devices.^{6,7} Thermal conductivity is one of the key material properties as it facilitates effective dissipation of heat, enabling lower cooling requirements and longer device lifetimes. Thermal energy is in semiconductors and insulators transferred primarily by phonon transport and is limited by phonon scattering processes. In addition to phonon-phonon and Umklapp scattering, scattering centers, such as point defects (ionized or neutral) and higher dimensional defects, like dislocations, can limit thermal conductivity. The dominant scattering mechanism depends on temperature: in the low temperature regime, dislocation and grain boundary scattering play important roles, while closer to the Debye temperature, point defect scattering becomes the predominant mechanism. ¹⁰ In this case, phonon scattering is a consequence of the breakdown of the crystal periodicity due to the presence of point defects. Point defects include the dopant atoms/ions, resulting in compensators that may be other impurities or vacancies, and their

complexes, which give rise to localized impurity states resonating with phonons. In general, point defect scattering is proportional to the corresponding defect size, mass, charge, and distribution and depends on their nature, i.e., substitutional or interstitial, impurities or vacancies, and isolated defects or defect complexes. 11-13 At higher temperatures, phonon-phonon scattering mechanisms determine the thermal conductivity, which converges to a single value almost independent of defects;¹⁴ typically, this happens above the room temperature, when the relaxation time is limited by phonon-phonon scattering rather than non-trivial phonon-defect scattering. 15 Consequently, the impact of point defects on the material's thermal performance during device operation has not been considered as a challenge. However, recent work has demonstrated that impurities play a significant role in determining the thermal conductivity even at room temperature. Zou et al. reported a decrease in the GaN thermal conductivity from 177 W/mK to 86 W/mK by increasing the Si concentration from 7×10^{16} to 5×10^{18} cm⁻³. ¹⁷ Jezowski *et al.* showed a maximum thermal conductivity of 1600 W/mK at 45 K in GaN with low concentrations of C, Si, and Mg. Kamatagi et al. investigated and modeled the influence of point defects on the thermal conductivity of GaN using

a) Author to whom correspondence should be addressed: pbagher@ncsu.edu

Sample	С	Mn	Fe	Other impurities	Total	κ at RT (W/mK)
Undoped	•••	•••	•••	$< 3 \times 10^{16}$	4×10^{16}	211 ± 5
Mn-doped	6×10^{16}	1×10^{18}		$< 2 \times 10^{17}$	1.3×10^{18}	212 ± 3
Fe-doped		3×10^{14}	1×10^{17}	$< 6 \times 10^{16}$	1.6×10^{17}	223 ± 4
C-doped	1×10^{18}	2×10^{16}	•••	$< 5 \times 10^{17}$	1.5×10^{18}	222 ± 4

TABLE I. SIMS concentrations (cm⁻³) and RT thermal conductivity (W/mK) of HVPE GaN samples with different dopants.

the Callaway model. Rounds *et al.* reported on the effects of different growth techniques and the corresponding incorporated point defects on the thermal conductivity of GaN. The room temperature thermal conductivity of GaN reported in the literature varies over a wide range, from 130 to 269 W m $^{-1}$ K $^{-1}$, 15 , $^{19-21}$ and depends on the growth methods and dominant impurities or defects.

Therefore, it is necessary to investigate the impact of point defects on the thermal conductivity of high-quality GaN single crystals to establish the influence of specific point defects or related mechanisms. Halide vapor phase epitaxy (HVPE) is an established growth technique, which yields high crystal quality GaN substrates with intended applications in high power electronics. Due to their high purity, HVPE crystals also exhibit a relatively high thermal conductivity, and in a recent comparison, unintentionally doped crystals exhibited the highest room temperature conductivity when compared to other growth techniques. Hence, HVPE GaN provides an ideal template to study the impact of doping with specific impurities on thermal conductivity due to a low background of unintentional impurities.

In this work, we describe a systematic study on the impact of specific impurities on the thermal conductivity of HVPE-grown single crystal GaN with an analysis based on the Debye–Callaway model that includes a Lorentzian oscillator-based impurity phonon resonance scattering. Substitutional impurities perturb the local potential energy, as they introduce a slight asymmetry in the host lattice. The changed potential energy landscape leads to modified interatomic forces that, in turn, induce observable resonances. ^{25,26} In the first part of this work, we study the impact of different impurities on the thermal conductivity with C, Fe, and Mn as dopants, followed by a study on the impact of the impurity concentration with a detailed study of Mn doping.

Bulk GaN samples were grown by HVPE on ammonothermal GaN substrates with a dislocation density (DD) of $5 \times 10^4 \, \mathrm{cm}^{-2}$ and were intentionally doped with C, Mn, and Fe with concentrations ranging from 10^{17} to $10^{19} \, \mathrm{cm}^{-3}.^{27,28}$ The 3ω method was employed to measure the thermal conductivity of GaN over a temperature ranging from $30 \, \mathrm{K}$ to $350 \, \mathrm{K}$. The measurement procedure is described elsewhere. 29,30 A Horiba XploRa PLUS Confocal Raman spectroscope with a laser wavelength of $532 \, \mathrm{nm}$ along with a Horiba Scientific CCD detector was used to investigate the vibrational modes of specific impurities.

The thermal conductivity of GaN single crystals grown by HVPE and intentionally doped with C, Mn, and Fe was investigated to distinguish between the effects arising due to the nature of the impurity and those related to the concentration. Table I shows the impurity concentrations, as measured by secondary ion mass spectroscopy (SIMS), and the corresponding thermal conductivities measured at room temperature for various dopants. Several general observations may be made:

(1) as discussed above, undoped HVPE GaN has a low concentration of background impurities (\sim 3 × 10¹⁶ cm⁻³), enabling controlled doping in a wide range to isolate the influence of the intended dopant; (2) undoped and low-doped GaN crystals exhibit similar thermal conductivity values at room temperature, independent of the impurity type or concentration; and (3) in contrast to room temperature, low temperature thermal conductivity values vary over a wide range, as shown in Fig. 1.

Figure 1 shows the measured thermal conductivity for various dopants in GaN, Mn ($1 \times 10^{18} \, \mathrm{cm}^{-3}$), Fe ($2 \times 10^{17} \, \mathrm{cm}^{-3}$), and C ($1 \times 10^{18} \, \mathrm{cm}^{-3}$), in the temperature range of 30–350 K. To understand the effects of dopants on GaN thermal conductivity, the Debye–Callaway model was utilized as described below, 14,31

$$\kappa = \frac{k_B^4 T^3}{2\pi^2 v \hbar^3} \left(\int_0^{\frac{\theta_D}{T}} \frac{\tau_C x^4 e^x}{(e^x - 1)^2} dx + \frac{\left(\int_0^{\frac{\theta_D}{T}} \frac{\tau_C x^4 e^x}{\tau_N (e^x - 1)^2} dx \right)^2}{\int_0^{\frac{\theta_D}{T}} \frac{\tau_C x^4 e^x}{\tau_N \tau_R (e^x - 1)^2 dx}} \right), \quad (1)$$

where $x=\frac{\hbar\omega}{k_BT}$, ν is the average speed of sound in the material, and $\theta_D=\frac{\hbar\omega_D}{k_B}$ and ω_D are the Debye temperature and frequency, respectively. τ_C , τ_N , and τ_R are combined, normal, and resistive relaxation times, respectively. The total resistive scattering rate is the sum of scattering rates from grain boundaries, τ_B^{-1} , impurities, and vacancies—based on the mass difference, impurity concentrations, τ_I^{-1} , and Umklapp processes, τ_{II}^{-1} ,

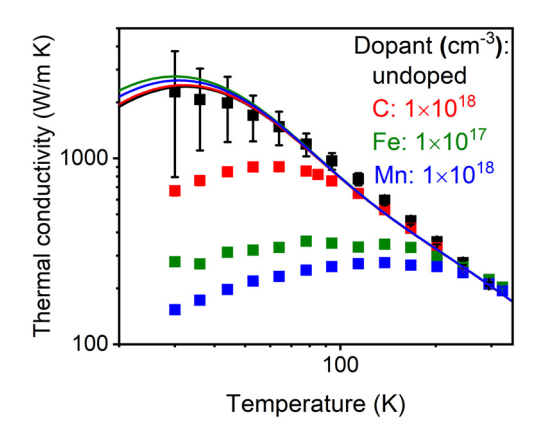


FIG. 1. Thermal conductivity curves for undoped, Mn-, Fe-, and C-doped HVPE GaN single crystals. Solid lines represent the Debye–Callaway-model. Error bars show the experimental error.

$$\tau_R^{-1} = \tau_B^{-1} + \tau_I^{-1} + \tau_U^{-1},\tag{2}$$

$$\tau_B^{-1} = \frac{\nu}{d},\tag{3}$$

$$\tau_I^{-1} = \frac{V}{4\pi \nu^3} \left(\frac{k_B}{\hbar}\right)^4 x^4 T^4 \Gamma_{isotopic},\tag{4}$$

$$\tau_U^{-1} = \frac{\hbar \gamma_G^2}{M \nu^2 \theta_D} \left(\frac{k_B}{\hbar}\right)^2 x^2 T^3 \exp\left(-\frac{\theta_D}{3T}\right),\tag{5}$$

where V, d, γ_G , and M are the volume per atom, characteristic length of the crystal, Grüneisen parameter, and average atomic mass of an atom in the host crystal, respectively. $\Gamma_{isotopic}$ is the mass-fluctuation phonon-scattering factor taking into the account the mass difference of the impurity atom and the host.³¹ The scattering rate due to the vacancies resembles τ_I^{-1} considering the absence of atoms.¹² Normal and combined scattering rates are

$$\tau_N^{-1} = \frac{k_B^3 \gamma_G^2 V}{M \hbar^2 \nu^5} \left(\frac{k_B}{\hbar}\right)^2 x^2 T^5, \tag{6}$$

$$\tau_C^{-1} = \tau_R^{-1} + \tau_N^{-1}. (7)$$

Another scattering mechanism is phonon-point defect scattering due to the disturbance of the host lattice by substitutional impurities. The scattering rate due to the elastic strain of impurities in the crystal mainly consists of the isotopic scattering factor ($\Gamma_{isotopic}$) and differences in stiffness constants and Pauling ionic radii of the impurity and the host atom. However, the latter parameters are negligible in comparison to the isotopic scattering factor for C, Fe, and Mn in GaN. Therefore, phonon-point defect scattering due to the stain field of impurities is mainly determined using Eq. (4), which is considered in the Debye–Callaway model.

The main contributions to the boundary scattering rate are the crystal dimensions and dislocations. The latter may be neglected due to the low threading dislocation density of $5\times 10^4\,\mathrm{cm}^{-2.36}$ Hence, with known crystal dimensions (Table II), impurity kind, and concentration, the boundary and impurity scattering rates can be calculated and the thermal conductivity can be predicted using the Debye–Callaway model. This is represented by the solid lines in Fig. 1. More details on the calculation procedure are found elsewhere, and the parameters used to predict thermal conductivity values based on the Debye–Callaway model are shown in Table II. The estimated vacancy concentrations in the range given in Table II and the variation of impurity concentrations ($\pm 1\times 10^{17}\,\mathrm{cm}^{-3}$) had an insignificant

TABLE II. Parameters used in the Debye–Callaway model for HVPE GaN. 15

Parameter	Value for HVPE GaN		
Vacancy concentration (cm ⁻³)	$1 \times 10^{17} - 1 \times 10^{19}$		
Phonon velocity (ms ⁻¹)	4759		
Debye temperature (K)	650		
Characteristic length (μm)	400-900		
Scattering factors	Based on impurity concentrations		
Grüneisen parameter	1.35		
Umklapp process rate constant, b	2		
Normal process coefficient	0.2		

impact on thermal conductivity predicted using the Debye-Callaway model.

Figure 1 shows that the Debye–Callaway model represents the thermal conductivity of undoped GaN relatively well over the whole temperature range. However, there is a significant deviation from the experimental data for the doped samples at low and intermediate temperatures. This deviation is more pronounced for Fe- and Mn-doped GaN. As discussed earlier, thermal conductivity at high temperatures is limited by Umklapp scattering, resulting in similar values for different samples. However, at lower temperatures, where thermal conductivity strongly depends on impurities, the Debye–Callaway model significantly overestimates the thermal conductivity of doped samples.

To better understand thermal conductivity at low temperatures, phonon resonances with specific impurities were considered.³⁷ In general, phonon scattering by impurities occurs due to (1) a time independent perturbation arising from the mass difference (also known as isotope scattering) and (2) time dependent oscillating harmonic perturbations arising from the vibrational modes associated with impurities. The latter is known as phonon-resonance scattering and can be modeled using a single Lorentz oscillator, which is expressed as follows:³⁷

$$\tau_{PR}^{-1} = \frac{A\left(\frac{\omega_0 \gamma}{2\pi^2}\right)\omega^2}{\left(\omega_0^2 - \omega^2\right)^2 + \left(\frac{\gamma}{\pi}\right)^2 \omega^2 \omega_0^2},\tag{8}$$

where constants A, ω_0 , and γ are a proportionality factor, the resonant angular frequency, and a damping factor, respectively. The resonant angular frequency, ω_0 , depends on the localized impurity state in the host and is a function of the mass difference between the impurity and host atom proportional to $\frac{1}{\sqrt{\mu}}$, where μ is the reduced mass. Resolved for the proportionality factor, A, is a function of the impurity concentration (density of oscillators) and the mass of the oscillator. The phonon resonance scattering rate τ^{-1}_{PR} is considered as an added resistive scattering rate in Eq. (2), and its contribution to the thermal conductivity can be calculated using the Debye–Callaway model [Eq. (1)].

As seen from Eq. (8), phonon resonance scattering is characterized by the phonon resonance frequency that corresponds to the local vibrational mode associated with a particular point defect, which, in this case, is an intentional impurity. Raman spectroscopy was employed to directly determine the resonance angular frequency for the mode of interest. Raman spectra of undoped and Mn-doped HVPE GaN single crystals, showing E^H₂ and A₁(LO), which are the characteristic GaN phonon modes, are shown in Fig. 2. A broad peak centered at 300 cm $^{-1}$ and corresponding to a localized energy resonant state ($\hbar\omega = 35 \,\mathrm{meV}$) was observed for Mn-doped GaN, consistent with previous identifications. 40,41 It is assumed that this energy approximates the phonon-defect resonance energy ω_0 for Mn-doped GaN. Other peaks in the Raman spectrum are GaN-related and independent of Mn. 40 Fe and C-related local vibrational modes were determined relative to the observed Mn-related Raman peak using the mass-difference approximation and assuming either Ga or N site occupation, respectively. 42 This procedure was used since no C- or Ferelated peaks were observed in the Raman spectra.³⁹ Accordingly,

$$\frac{\omega_C}{\omega_{Mn}} \propto \sqrt{\frac{\mu_{MnN}}{\mu_{GaC}}} \tag{9}$$

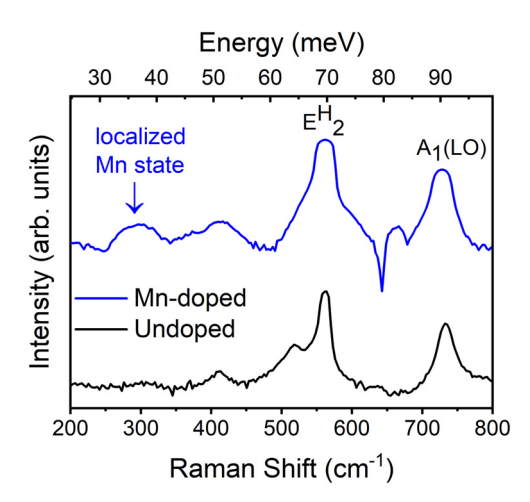


FIG. 2. Raman spectrum of undoped and Mn-doped HVPE GaN with a Raman shift at 300 cm⁻¹, indicating a Mn localized state.

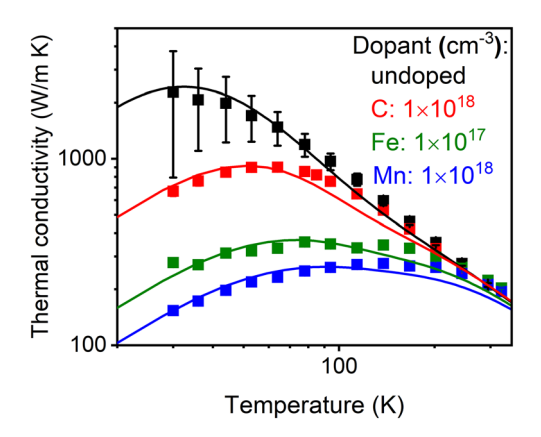


FIG. 3. Fitting curves for the modified Callaway model considering single mode Lorentz oscillators to account for phonon resonances with 37, 35, and 35 meV as resonance energies for C, Mn, and Fe, respectively. The proportionality factor, A, is the fitting parameter.

and

$$\frac{\omega_{Fe}}{\omega_{Mn}} \propto \sqrt{\frac{\mu_{MnN}}{\mu_{FeN}}},\tag{10}$$

where $\frac{1}{\mu_{ij}} = \frac{1}{m_i} + \frac{1}{m_j}$ is the reduced mass. It is clear that metals occupying the Ga site, Mn_{Ga} ($m_{Mn} = 54.94$ g/mol and $\mu = 11.16$ g/mol) and

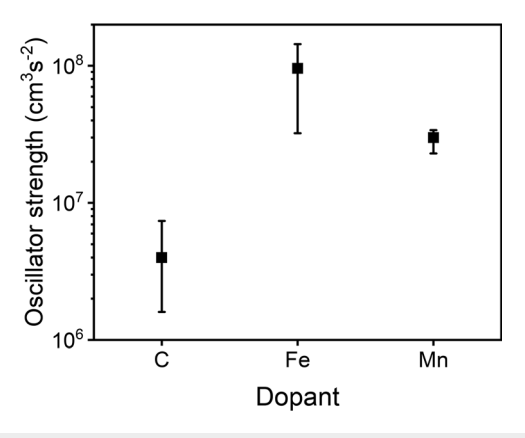


FIG. 4. Oscillator strength f extracted from proportionality factor A by considering phonon resonances in the Callaway model. Error bars indicate the propagation of uncertainty due to the fitting parameter A and variation of impurity concentrations $(\pm 1 \times 10^{17} \, \text{cm}^{-3})$.

 Fe_{Ga} ($m_{Fe} = 55.84$ g/mol and $\mu = 11.2$ g/mol), are expected to show similar localized vibrational modes at 35 meV, which is similar to the Mn localized state and close to the experimental values previously reported for the Fe impurities in GaN.⁴³ C_N ($m_C = 12.01$ g/mol and $\mu = 10.25$ g/mol), with a slightly lower reduced mass, is expected to have a vibrational mode at 37 meV. Based on the measured and estimated resonance energies for the single oscillator Lorentz model and employing the proportionality factor (dependent on the impurity concentration and oscillator strength) as a fitting parameter, the experimental thermal conductivities were fitted using a modified Callaway model, as shown in Fig. 3. The damping factor, γ , was considered as a constant equal to one as it does not significantly influence the fitting results.³⁷ The oscillator strength, f = A/(impurity concentration), for different impurities is shown in Fig. 4. Since the reduced masses for Mn and Fe are similar, they have similar oscillator strengths. As expected, C, with the lowest oscillator strength, shows the smallest impact of phonon resonances on thermal conductivity. Although, C is an amphoteric impurity, C_{Ga} with $m_C = 12.01$ g/mol and $\mu = 6.466$ g/mol, resulting in a resonance energy of 45 meV, would have a much lower influence on thermal conductivity than C_N.

Finally, the effect of the impurity concentration on thermal conductivity is investigated for HVPE GaN doped with Mn in the range of 1×10^{18} – $2\times10^{19}\,\mathrm{cm}^{-3}$. All Mn-doped crystals showed broad Raman peaks centered at 35 meV, independent of the doping level. Table III shows Mn concentrations and corresponding RT thermal conductivities. Low-doped GaN crystals exhibit similar thermal conductivity values at room temperature as the samples in Table I. Only

TABLE III. SIMS impurity concentrations (cm⁻³) of Mn-doped HVPE GaN samples and corresponding thermal conductivity values at RT.

Sample	С	Mn	Fe	Other impurities	Total	κ at RT (W/mK)
Mn-doped 1	6×10^{16}	1×10^{18}		$< 2 \times 10^{17}$	1.3×10^{18}	212 ± 3
Mn-doped 2	2×10^{16}	2×10^{18}		$< 2 \times 10^{17}$	2.3×10^{18}	222 ± 3
Mn-doped 3		1×10^{19}	1×10^{16}	$< 5 \times 10^{16}$	1×10^{19}	180 ± 4
Mn-doped 4		2×10^{19}		$< 6 \times 10^{16}$	2×10^{19}	151 ± 2

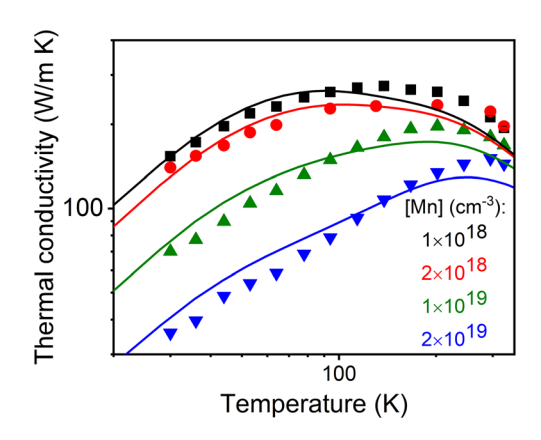


FIG. 5. Thermal conductivity curves for different Mn doping concentrations: symbols represent measurements, and solid lines correspond to fitting curves using the modified Callaway model.

when the impurity concentration exceeds $\sim 10^{19}\,\mathrm{cm}^{-3}$, a significant reduction in RT thermal conductivity ensues. As seen in Fig. 5, increasing the Mn concentration reduces the thermal conductivity for all temperatures, showing the importance of phonon resonances at practical device operating temperatures and doping levels. A small deviation of the modified model from experimental results seems to be due to the presence of other Mn-related states.

Similar to Fig. 3, the proportionality factor, A, was extracted as the best fit to the experimental data using the resonant 35 meV transition. The oscillator strength remained constant, within the experimental error, for all Mn concentrations, and the proportionality factor was proportional to the oscillator density.

In conclusion, the thermal conductivity of GaN strongly depends on the type of dopants and concentration. The influence of dopants was modeled using a modified Debye–Callaway model, wherein the impurity scattering was described using a Lorentz oscillator. Based on Raman measurements, the resonance energy for Mn was found to be 35 meV; the corresponding resonant frequencies for C and Fe were calculated using the mass-difference approximation. While room temperature thermal conductivity remained high for the low-doped samples, increasing the Mn doping concentration to $2\times 10^{19}~{\rm cm}^{-3}$ decreased TC to $\sim\!\!2/3$ of the original value.

The authors acknowledge funding in part from the NSF (Nos. ECCS-1508854, ECCS-1610992, DMR-1508191, and ECCS-1653383), ARO (W911NF-15-2-0068 and W911NF-16-C-0101), the AFOSR (No. FA9550-17-1-0225), the DOE (No. DE-SC0011883), and the ONRG NICOP (No. N62909-17-1-2004).

DATA AVAILABILITY

The data that support the findings of this study are available within the article.

REFERENCES

- ¹B. J. Baliga, Semicond. Sci. Technol. **28**, 074011 (2013).
- ²S. Chowdhury, B. L. Swenson, M. H. Wong, and U. K. Mishra, Semicond. Sci. Technol. 28, 074014 (2013).
- ³J. Y. Tsao, S. Chowdhury, M. A. Hollis, D. Jena, N. M. Johnson, K. A. Jones, R. J. Kaplar, S. Rajan, C. G. V. de Walle, E. Bellotti, C. L. Chua, R. Collazo, M. E.

- Coltrin, J. A. Cooper, K. R. Evans, S. Graham, T. A. Grotjohn, E. R. Heller, M. Higashiwaki, M. S. Islam, P. W. Juodawlkis, M. A. Khan, A. D. Koehler, J. H. Leach, U. K. Mishra, R. J. Nemanich, R. C. N. Pilawa-Podgurski, J. B. Shealy, Z. Sitar, M. J. Tadjer, A. F. Witulski, M. Wraback, and J. A. Simmons, Adv. Electron. Mater. 4, 1600501 (2018).
- ⁴P. Reddy, B. Sarkar, F. Kaess, M. Gerhold, E. Kohn, R. Collazo, and Z. Sitar, Appl. Phys. Lett. **110**, 011603 (2017).
- ⁵I. C. Kizilyalli, A. P. Edwards, H. Nie, D. Disney, and D. Bour, IEEE Trans. Electron Devices **60**, 3067 (2013).
- ⁶E. A. Jones, F. F. Wang, and D. Costinett, IEEE J. Emerg. Sel. Top. Power Electron. 4, 707 (2016).
- ⁷A. M. Ozbek and B. J. Baliga, IEEE Electron Device Lett. **32**, 300 (2011).
- ⁸T. P. Chow and R. Tyagi, IEEE Trans. Electron Devices **41**, 1481 (1994).
- ⁹A. Jeżowski, B. A. Danilchenko, M. Boćkowski, I. Grzegory, S. Krukowski, T. Suski, and T. Paszkiewicz, Solid State Commun. 128, 69 (2003).
- ¹⁰P. D. Thacher, Phys. Rev. **156**, 975 (1967).
- ¹¹D. C. Larsen, *Thermal Conductivity* (Springer Science & Business Media, 2012), Vol. 16.
- ¹²C. A. Ratsifaritana and P. G. Klemens, Int. J. Thermophys. 8, 737 (1987).
- ¹³G. A. Slack, Phys. Rev. **126**, 427 (1962).
- 14T. M. Tritt, Thermal Conductivity: Theory, Properties, and Applications (Springer Science & Business Media, 2006).
- 15 R. Rounds, B. Sarkar, T. Sochacki, M. Bockowski, M. Imanishi, Y. Mori, R. Kirste, R. Collazo, and Z. Sitar, J. Appl. Phys. 124, 105106 (2018).
- ¹⁶Q. Zheng, C. Li, A. Rai, J. H. Leach, D. A. Broido, and D. G. Cahill, Phys. Rev. Mater. 3, 014601 (2019).
- ¹⁷J. Zou, D. Kotchetkov, A. A. Balandin, D. I. Florescu, and F. H. Pollak, J. Appl. Phys. **92**, 2534 (2002).
- ¹⁸M. D. Kamatagi, N. S. Sankeshwar, and B. G. Mulimani, Diamond Relat. Mater. 16, 98 (2007).
- ¹⁹ A. Jeżowski, O. Churiukova, J. Mucha, T. Suski, I. A. Obukhov, and B. A. Danilchenko, Mater. Res. Express 2, 085902 (2015).
- ²⁰E. K. Sichel and J. I. Pankove, J. Phys. Chem. Solids 38, 330 (1977).
- ²¹A. Jeżowski, P. Stachowiak, T. Plackowski, T. Suski, S. Krukowski, M. Boćkowski, I. Grzegory, B. Danilchenko, and T. Paszkiewicz, Phys. Status Solidi B 240, 447 (2003).
- ²²R. P. Tompkins, M. R. Khan, R. Green, K. A. Jones, and J. H. Leach, J. Mater. Sci. Mater. Electron. 27, 6108 (2016).
- O. Aktas and I. C. Kizilyalli, IEEE Electron Device Lett. 36, 890 (2015).
- ²⁴J. Suda, K. Yamaji, Y. Hayashi, T. Kimoto, K. Shimoyama, H. Namita, and S. Nagao, Appl. Phys. Express 3, 101003 (2010).
- ²⁵D. Mills, J. Phys. Colloq. **28**(C1), C1-3 (1967).
- ²⁶B. Dongre, J. Carrete, A. Katre, N. Mingo, and G. K. H. Madsen, J. Mater. Chem. C 6, 4691 (2018).
- ²⁷M. Iwinska, M. Zajac, B. Lucznik, M. Fijalkowski, M. Amilusik, T. Sochacki, E. Litwin-Staszewska, R. Piotrzkowski, I. Grzegory, and M. Bockowski, Jpn. J. Appl. Phys., Part 1 58, SC1047 (2019).
- ²⁸M. Iwinska, R. Piotrzkowski, E. Litwin-Staszewska, T. Sochacki, M. Amilusik, M. Fijalkowski, B. Lucznik, and M. Bockowski, Appl. Phys. Express 10, 011003 (2017).
- ²⁹D. G. Cahill, Rev. Sci. Instrum. **61**, 802 (1990).
- ³⁰D. G. Cahill and R. O. Pohl, Phys. Rev. B **35**, 4067 (1987).
- ³¹D. T. Morelli, J. P. Heremans, and G. A. Slack, Phys. Rev. B 66, 195304 (2002).
- ³²P. P. Paskov, M. Slomski, J. H. Leach, J. F. Muth, and T. Paskova, AIP Adv. 7, 095302 (2017).
- ³³B. Abeles, Phys. Rev. **131**, 1906 (1963).
- ³⁴D. Wickramaratne, J.-X. Shen, C. E. Dreyer, A. Alkauskas, and C. G. Van de Walle, Phys. Rev. B 99, 205202 (2019).
- 35J. L. Lyons, A. Janotti, and C. G. Van de Walle, Phys. Rev. B 89, 035204 (2014).
- 36C. Mion, J. F. Muth, E. A. Preble, and D. Hanser, Appl. Phys. Lett. 89, 092123
- ³⁷R. O. Pohl, Phys. Rev. Lett. **8**, 481 (1962).
- ³⁸Y. H. Zhang, L. L. Guo, and W. Z. Shen, Mater. Sci. Eng., B 130, 269 (2006)

³⁹A. Kaschner, H. Siegle, G. Kaczmarczyk, M. Straßburg, A. Hoffmann, C. Thomsen, U. Birkle, S. Einfeldt, and D. Hommel, Appl. Phys. Lett. 74, 3281

⁴⁰ W. Gebicki, J. Strzeszewski, G. Kamler, T. Szyszko, and S. Podsiadło, Appl. Phys. Lett. 76, 3870 (2000).

X. G. Cui, Z. K. Tao, R. Zhang, X. Li, X. Q. Xiu, Z. L. Xie, S. L. Gu, P. Han, Y. Shi, and Y. D. Zheng, Appl. Phys. Lett. 92, 152116 (2008).
C. G. Van de Walle and J. Neugebauer, J. Appl. Phys. 95, 3851 (2004).
C. Göbel, C. Schrepel, U. Scherz, P. Thurian, G. Kaczmarczyk, and A. Hoffmann, Mater. Sci. Forum 258-263, 1173 (1997).